Mitochondrion

Identification of a Novel m.3955G>A Variant in MT-ND1 Associated with Leigh Syndrome

--Manuscript Draft--

Manuscript Number:	MITOCH-D-21-00164R1
Article Type:	Research Paper
Section/Category:	
Keywords:	Novel mitochondiral DNA variant; MT-ND1; Leigh syndrome; cybrid cells
Corresponding Author:	Manting Xu Capital Medical University Affiliated Beijing Children's Hospital China
First Author:	Manting Xu, Dr
Order of Authors:	Manting Xu, Dr
	robert Kopajtich
	Matthias Elstner
	Hua Li
	Zhimei Liu
	Junling Wang
	prokisch Holger
	Fang Fang
Abstract:	Leigh syndrome (LS) is one of the most common mitochondrial diseases in children, for which at least 90 causative genes have been identified. However, many LS patients have no genetic diagnosis, indicating that more disease-related genes remain to be identified. In this study, we identified a novel variant, m.3955G>A, in mitochondrially encoded NADH:ubiquinone oxidoreductase core subunit 1 (MT-ND1) in two unrelated LS patients, manifesting as infancy-onset frequent seizures, neurodegeneration, elevated lactate levels, and bilateral symmetrical lesions in the brainstem, basal ganglia, and thalamus. Transfer of the mutant mtDNA with m.3955G>A into cybrids disturbed the MT-ND1 expression and CI assembly, followed by remarkable mitochondrial dysfunction, reactive oxygen species production, and mitochondrial membrane potential reduction. Our findings demonstrated the pathogenicity of the novel m.3955G>A variant, and extend the spectrum of pathogenic mtDNA variants.
Suggested Reviewers:	Michelangelo Mancuso mancusomichelangelo@gmail.com
	Häberle Johannes Johannes.Haeberle@kispi.uzh.ch
	Costanza Lamperti Costanza.Lamperti@istituto-besta.it
	Agnès Rötig agnes.rotig@inserm.fr
	Chuanzhu Yan czyan@sdu.edu.cn
	Minxin Guan gminxin88@zju.edu.cn
	Kei Murayama kmuraya@mri.biglobe.ne.jp
Response to Reviewers:	

Highlights

We identified a novel pathogenic variant in the *MT-ND1* gene (m.3955G>A, p.A217T) in two unrelated Leigh Syndrom patients.

Clinical analyses, and biochemical investigations supported the pathogenicity of the detected variant.

Our findings demonstrated the pathogenicity of the novel m.3955G>A variant, and extend the spectrum of pathogenic mtDNA variants.

Identification of a Novel m.3955G>A Variant in *MT-ND1* Associated with Leigh Syndrome

Manting Xu[1], Robert Kopajtich[2, 3], Matthias Elstner[4], Hua Li[1], Zhimei Liu[1], Junling Wang[1], Holger Prokisch[2, 3], Fang Fang[1*]

[1]Department of Neurology, Beijing Children's Hospital, Capital Medical University, National Center for Children's Health, Beijing 100045, China,

[2]Institute of Human Genetics, Technical University of Munich, Munich 81675, Germany;

[3]Institute of Neurogenomics, Helmholtz Zentrum München, Munich 85764, Germany

[4]Department of Neurology, Technical University of Munich, School of Medicine, Munich 81675, Germany

* To whom correspondence should be addressed:

Prof. Fang Fang

Tel: 0086 13910150389

E-mail: fangfang@bch.com.cn

Abstract

Leigh syndrome (LS) is one of the most common mitochondrial diseases in children, for which at least 90 causative genes have been identified. However, many LS patients have no genetic diagnosis, indicating that more disease-related genes remain to be identified. In this study, we identified a novel variant, m.3955G>A, in mitochondrially encoded NADH:ubiquinone oxidoreductase core subunit 1 (*MT-ND1*) in two unrelated LS patients, manifesting as infancy-onset frequent seizures, neurodegeneration, elevated lactate levels, and bilateral symmetrical lesions in the brainstem, basal ganglia, and thalamus. Transfer of the mutant mtDNA with m.3955G>A into cybrids disturbed the MT-ND1 expression and CI assembly, followed by remarkable mitochondrial dysfunction, reactive oxygen species production, and mitochondrial membrane potential reduction. Our findings demonstrated the pathogenicity of the novel m.3955G>A variant, and extend the spectrum of pathogenic mtDNA variants.

Keywords: Novel mitochondrial DNA variant; *MT-ND1*; Leigh syndrome; cybrid cells

Introduction

Leigh syndrome (LS; MIM 256000), also known as subacute necrotizing encephalomyelopathy, is one of the most common mitochondrial diseases in children, with an estimated prevalence of 1 per 40,000 live births. LS generally presents as neurological symptoms in early childhood, including developmental delays or regression, hypotonia, ataxia, dystonia, and ophthalmological abnormalities including nystagmus and optic atrophy(Lake et al., 2016). Multisystemic presentations including cardiac, hepatic, gastrointestinal, and renal tubular dysfunction have been observed(Sofou et al., 2014). Bilateral symmetrical lesions within the brainstem and basal ganglia are characteristic neuroradiological features of LS(Arii et al., 2000). Evidence indicating abnormal energy metabolism, such as a defect in oxidative phosphorylation or pyruvate dehydrogenase complex activity, or an elevated serum or cerebrospinal fluid (CSF) lactate level, is also a criterion for the diagnosis of LS(Baertling et al., 2014). Pathogenic variants in both the mitochondrial and nuclear genome have been identified in at least 90 genes in LS patients, and mitochondrial DNA (mtDNA) variants are responsible for 10–20% of LS cases. However, many LS patients have no genetic diagnosis, indicating that more disease-related genes remain to be identified(Lake et al., 2016; Rahman et al., 2017).

Mitochondrial complex I (CI), a large membrane protein complex of the respiratory chain, oxidizes NADH to reduce ubiquinone and is coupled with proton translocation across the mitochondrial inner membrane. CI, which contains a hydrophilic peripheral arm and a hydrophobic membrane arm, consists of 7 subunits

encoded by mtDNA and 38 subunits encoded by nuclear DNA (nDNA)(Zickermann et al., 2015; Parey et al., 2020). Mitochondrially encoded NADH: ubiquinone oxidoreductase core subunit 1 (MT-ND1), located at the proximal end of the membrane arm, provides the docking site for the Q module of CI. Due to the crucial functions of CI in the respiratory chain, it accounts for most cases of respiratory chain deficiency in humans, with defects resulting in a wide range of clinical presentations, including LS(Lightowlers et al., 2015).

Here, we report two unrelated LS patients harboring the same novel m.3955G>A variant in *MT-ND1*. We confirmed the pathogenicity and molecular pathomechanisms of this variant via a combination of clinical analyses, genetic analyses, and transmitochondrial cybrid cell studies.

2. Subjects and methods

2.1 Subjects

Patient 1 The third child of healthy non-consanguineous Chinese parents was born with a normal birth weight, height, and head circumference following an uneventful pregnancy and term delivery. The family history was unremarkable. From the age of 7 months, he began to suffer intermittent seizures (including myoclonus, spasms, and focal motor seizures), developmental regression, ptosis, dystonia, night apnea, and swallowing dysfunction. Laboratory parameters showed that the serum and CSF lactate levels were high at 6.3 and 4.2 mmol/L (normal level < 2.8 mmol/L), respectively. Additional laboratory results including the blood cell count, serum levels of creatine kinase and ammonia, liver and kidney function tests, and CSF cell counts and protein

levels were all within normal ranges. Brain magnetic resonance imaging (MRI) at 7 months of age revealed bilateral symmetrical lesions with increased T2 signals in the brainstem, basal ganglia, and thalamus. Brain MRI repeated at 4.5 years of age showed similar symmetrical lesions as previously observed, increased T2 signals in the temporoparietal cortex, and cerebral atrophy (Fig. 1A). Electroencephalography (EEG) recorded multifocal high-amplitude epileptic discharges in the frontal, occipital, and temporal regions. Slow background waves and a seizure episode were also recorded (Fig. 1B). No abnormality upon hematoxylin and eosin (H&E), modified Gomori trichrome (MGT), cytochrome c oxidase (COX), and succinate dehydrogenase (SDH) staining was detected in a muscle biopsy sample derived from the right biceps of the patient. Levetiracetam, nitrate diazepam, and multivitamins (dosages unknown) were prescribed. The seizures were reduced by 30–40%, whereas the other manifestations described above exhibited no improvements.

Patient 2 The second child of healthy non-consanguineous Chinese parents was born after 41 weeks of gestation by cesarean delivery with a normal birth weight, height, and head circumference. The family history was unremarkable. Since the age of 1 month, the patient presented with a developmental delay. Intermittent seizures (including spasms and tonic seizures) ensued from the age of 5 months. His serum and CSF lactate levels were high at 7.2 and 4.6 mmol/L (normal level < 2.8 mmol/L), respectively. Laboratory results including levels of serum creatine kinase, serum ammonia, and carnitine were normal. Brain MRI revealed bilateral symmetrical lesions in the thalamus, basal ganglia, and brainstem on T2- and diffusion-weighted imaging.

Abnormal signals were also detected in the frontotemporal lobe in T2/FLAIR images (Fig. 2A). EEG revealed hypsarrhythmia and a burst-suppression pattern in the interictal period, as well as several episodes of seizures (Fig. 2B). No abnormality was detected upon H&E, MGT, COX, and SDH staining of a muscle biopsy sample derived from the right biceps of the patient. At 11 months of age, the patient experienced status epilepticus following a respiratory infection and died within 12 h.

2.2 Molecular genetic analyses

Total nDNA was extracted from circulating lymphocytes, and mtDNA was extracted from circulating lymphocytes, urinary sediment, hair follicles, fingernail cells, and fibroblasts using standard methodologies(Ji et al., 2014). Entire mtDNA next-generation sequencing and whole exome sequencing were performed to detect causative variants (HiSeq X Ten sequencer, Illumina, San Diego, CA, USA). Sanger sequencing was conducted using 2× Taq Master Mix (Thermo Fisher Scientific, Waltham, MA, USA) and Applied Biosystems thermal cyclers (Applied Biosystems, Foster City, CA, USA)(Grady et al., 2018).

The MutPred score(Pejaver et al., 2020), PolyPhen-2(Adzhubei et al., 2013), and PROVEAN(Choi et al., 2015) were used to predict the potential impact of amino-acid substitutions on the stability and function of the MT-ND1 protein. The structure of human MT-ND1 was analyzed based on a cryogenic electron microscopy (Cryo-EM) structure of human CI at 3.7 Å resolution (PDB ID: 5XTD). PyMOL (PyMOL Molecular Graphics System V 2.4.0a0) was used to visualize the protein structure and model amino-acid changes in three-dimensional view.

2.3 Generation of transmitochondrial cybrids

To generate transmitochondrial cybrid cells with the m.3955G>A variant, platelets from blood samples of patient 1 were fused with human osteosarcoma 143B cells lacking mtDNA as previously described(Chomyn, 1996). The cybrid clones were cultured in Dulbecco's modified Eagle medium (Thermo Fisher Scientific) supplemented with 1% penicillin and 10% fetal bovine serum (both Thermo Fisher Scientific) at 37°C and 5% CO_2. Cybrid clones with the m.3955G>A variant (mutant) and lacking this variant (wild-type) were selected for further experiments.

2.4 Western blotting and blue native polyacrylamide gel electrophoresis

Western blotting was carried out as previously described(Ji et al., 2020). Briefly, protein extracted from cybrids and fibroblast cells derived from patient 1 and his mother was separated using sodium dodecyl sulfate-polyacrylamide gel electrophoresis (PAGE) and transferred onto polyvinylidene difluoride membranes. The membranes were blocked in 5% milk for 1 h and incubated overnight at 4℃ with anti-MT-ND1 (ab181848; Abcam, Cambridge, UK), anti-MT-ND4 (A9941, Abclonal, Shanghai, China), anti-MT-ND5 (ab230509, Abcam), and NDUFB8 (ab192878, Abcam) as the primary antibody and anti-VDAC (4661; Cell Signaling Technology, Danvers, MA, USA) serving as the control(Ji et al., 2020). Blue native-PAGE was performed with mitochondrial proteins from cybrids as previously described(Delmiro et al., 2013) using antibodies against NDUFS2 (ab110249; Abcam), SDHA (ab14715; Abcam), UQCRC2 (ab14745; Abcam), MT-COXIV (ab202554; Abcam), ATPB (ab14730; Abcam), and VDAC (4661; Cell Signaling Technology).

2.5 Respiratory chain enzyme activity assays

The activities of mitochondrial respiratory chain (MRC) complexes and the mitochondrial marker citrate synthase (CS) were assayed in isolated mitochondria obtained from cybrid cells, as previously described(Ogawa et al., 2017). The enzyme activities of CI; complexes II, II+III, and IV; and CS are presented as percentages relative to the activities of reference enzymes(Ogawa et al., 2017).

2.6 Measurement of oxygen consumption rate

The measurements of oxygen consumption rate (OCR) in cybrid cells were performed using the XF96 Extracellular Flux Analyzer (Agilent Technologies, Santa Clara, CA, USA), as detailed previously(Kremer et al., 2017; Ogawa et al., 2017). Cells were seeded at a density of 2×10^4 cells per well in Seahorse XF96 polystyrene cell culture plates (Agilent Technologies).

The following inhibitors were used in mitochondrial stress tests: 1 μM oligomycin A, 0.5 μM carbonyl cyanide 4-trifluoromethoxy-phenylhydrazone (FCCP), 1 μM rotenone, and 1 μM antimycin A. The assay medium and inhibitors used in the mitochondrial stress tests were adjusted to pH 7.4. The following inhibitors were used in the MRC complex assays: 2 μM rotenone, 10 mM succinate, 5 μM antimycin A, 10 mM ascorbate, and 0.5 mM Wurster's blue. All solutions and injections in the MRC complex assays were maintained at a pH of 7.2(Qian et al., 2019).

2.7 Measurement of mitochondrial reactive oxygen species production

The reactive oxygen species (ROS) were measured with MitoSOX™ Red (M36008; Molecular Probes, Eugene, OR, USA) as previously described(Jia et al., 2019). Cybrid

cells were incubated for 24 h and stained with MitoSOX, MitoTracker™ Green (M7514, Molecular Probes, USA) and Hochest (C1022; Beyotime Biotechnology, Beijing, China) in the dark. After incubation (37°C, 5% CO_2) for 20 min, the cybrid cells were washed and resuspended in phosphate-buffered saline (PBS). Images were taken using an LSM 780 confocal microscope (Zeiss, Germany). MitoSOX Red was detected at an excitation wavelength of 510 nm and an emission wavelength of 580 nm, and the fluorescence intensity was evaluated using ImageJ software.

2.8 Measurement of mitochondrial membrane potential

The mitochondrial membrane potential (MMP) was measured using a fluorescence-based JC-1 assay kit (C2006; Beyotime Biotechnology). Cybrid cells were grown for 24 h and incubated (37°C, 5% CO_2) in culture medium supplemented with JC-1 and Hochest (C1022; Beyotime Biotechnology in the dark. After 20 min, the cybrids were washed twice with PBS, and JC-1 fluorescence was measured using an LSM 780 confocal microscope (Zeiss, Germany). JC-1 aggregates and monomers were detected at excitation/emission wavelengths of 585/590 and 514/529 nm, respectively and the fluorescence intensity was evaluated using ImageJ software.

2.9 Statistical analyses

Statistical parameters are presented in the figure legends. The data from *in vitro* experiments were derived from at least three replicate experiments. Normally distributed data were analyzed via one-way analysis of variance (ANOVA) followed by Tukey's honestly significant difference *post hoc* test using Prism 8.0 for Windows (GraphPad software, Inc., San Diego, CA, USA). A *p-value* < 0.05 was considered to

indicate statistical significance.

3. Results

3.1. Detection of a novel variant in *MT-ND1*

Based on the clinical characteristics, the two patients were confirmed to have LS. However, no known pathogenic mtDNA variant was detected via mitochondrial gene sequencing, and no potential biallelic variant of any gene associated with mitochondrial disease was detected via whole exome sequencing.

The novel heteroplasmic G-to-A transition at nucleotide 3955 of *MT-ND1* was detected in the two patients via complete mitochondrial gene sequencing. This variant resulted in a substitution of alanine at position 217 to threonine (p.A217T) in *MT-ND1*. In patient 1, the m.3955G>A/*MT-ND1* variant exhibited heteroplasmy in different tissues, with mutation loads of 86.3%, 92.7%, 77.0%, 89.2%, and 68.7% in the circulating leukocytes, urinary sediment, hair follicles, fibroblasts, and fingernail cells, respectively. DNA samples obtained from the maternal family members (including the patient's mother and two older sisters) of patient 1 revealed no m.3955G>A variant in the urinary sediment, hair follicles, fingernail cells, fibroblasts (obtained only from the patient's mother), or blood samples, indicating that the variant had arisen *de novo* during embryogenesis and had not been maternally inherited (Fig 3A).

The m.3955G>A variant was also detected in the circulating leukocytes of patient 2, with a mutation load of 90.7%. The variant was absent in the circulating leukocytes of this patient's maternal family members (including the patient's mother and older brother) (Fig 3A). No other suspected pathogenic variants were detected via complete mtDNA sequencing in the DNA samples of the two patients (Supplemental table 1-2).

Phylogenetic conservation analyses of the MT-ND1 protein sequence from 12 species

revealed that the alanine residue at position 217 is highly conserved (Fig. 3B). The MutPred score was 0.736, which exceeds the threshold required to distinguish the variant from polymorphic changes(Pejaver et al., 2020). The PolyPhen-2 score was 1.000, which predicted the variant to be "probably damaging"(Adzhubei et al., 2013). The PROVEAN score was –2.68, predicting that the variant would have a "deleterious" effect on protein function(Choi et al., 2015).

The Cryo-EM structure of MT-ND1 in human CI was examined to analyze the effects caused by this variant. In close-up view, alanine-217 is located at the mitochondrial matrix side of MT-ND1, the main region of contact with the Q module of the peripheral arm. The substitution of alanine at this position gives rise to steric hindrance with the adjacent domain and increases the likelihood of van der Waals energy clashes, which is predicted to destabilize MT-ND1 and likely disturb CI assembly and function (Fig 3C).

3.2. The m.3955G>A variant reduces the level of mitochondrial proteins

Western blot analysis showed that the levels of MT-ND1 were significantly reduced in the two mutant cybrid cell lines (M1 and M2, with mutation loads of 87.2% and 97.9%, respectively) compared with wild-type cybrid cells (WT) (Fig. 4A). The expression of MT-ND1 was significantly reduced in the fibroblast cells derived from patient 1 compared with those from his mother (Fig. 4B).

To determine whether the m.3955G>A variant may impair the expression of other CI subunits, the levels of two mtDNA-encoded CI subunits and a nDNA-encoded CI subunit were evaluated. The expression levels of these CI proteins, probed by antibodies against MT-ND4, MT-ND5 and NDUFB8 were also significantly reduced.

Furthermore, we investigated the possible role played by the m.3955G>A variant in MRC complex assembly. The amount of mature CI in M1 and M2 clones was significantly reduced compared with WT cybrid cells (Fig. 4B); all other complexes

were expressed at similar levels in M1 and M2 clones compared with WT cybrid cells, indicating that this variant affected the assembly of CI.

3.3.The m.3955G>A variant results in mitochondrial respiration deficiency

The basal OCRs of M1 and M2 cybrid cell lines were significantly reduced to 54.0% and 53.7% of the mean value measured in WT cybrid cells. Electron transport chain inhibitors or uncoupling agents were also used to further assess cellular bioenergetic activities. The ATP-linked OCRs of M1 and M2 cybrid cell lines were significantly reduced to 49.0% and 48.6%, their maximal OCRs were significantly reduced to 60.5% and 51.3%, and the reserve capacity OCRs were significantly reduced to 68.0% and 47.2%, respectively. The proton leakage and non-mitochondrial OCRs in both mutant cybrid cell lines were close to those of WT cybrids (Fig 5A).

To fully assess the impact of this variant on the activities of the MRC complexes, we evaluated the complex I-, II-, and IV-mediated OCRs in cybrid cells. The M1 and M2 cybrid cell lines exhibited significant decreases in the CI-mediated OCR relative to wlid-type cybrid cells (37% and 31.3%, respectively). The complex II- and IV-mediated OCRs in mutant cybrid cell lines were comparable to those of the wlid-type cybrid cells (Fig 5B).

We used a biochemical assay to determine the activities of the MRC complexes. Consistently, the relative CI enzyme activities of the M1 and M2 clones were significantly reduced compared with the WT cybrid cells ($p < 0.05$). However, the complex-II, -II+III, -III, and IV activities in mutant cybrids cell lines were comparable to those in the wlid-type cybrid cells (Table 1).

3.4 The m.3955G>A variant increases the production of mitochondrial ROS

The results of the MitoSOX Red assay are shown in Figure 6A–6B. The intensity of red fluorescence in the mutant cybrid cell lines was significantly higher than that in WT

cybrid cells, indicating that ROS generation in mutant cybrid cell lines carrying the m.3955G>A variant was significantly increased.

3.5 The m.3955G>A variant reduces the MMP

The MMP was measured in cybrid cells using JC-1. Staining and imaging analyses showed that JC-1 formed red fluorescent aggregates in WT cybrid cells, indicating that JC-1 had accumulated in polarized mitochondrial membranes, whereas in the mutant cybrid cells, JC-1 existed in a monomeric form and stained the cells green, indicating a decreased MMP (Fig 7A). The ratios of red to green fluorescence in M1 and M2 cybrid cell lines carrying the m.3955G>A variant were significatly lower compared with that in WT cybrid cells (Fig 7B), indicating that the MMPs in m.3955G>A mutant cybrid cells were significantly reduced.

Discussion

In this study, we identified a novel pathogenic variant, m.3955G>A (p.A217T) in *MT-ND1* in two unrelated young males, both patients manifesting as infancy-onset frequent seizures, neurodegeneration, elevated lactate levels, and bilateral symmetrical lesions in the brainstem, basal ganglia, and thalamus, fulfilling the diagnostic criteria for LS(Baertling et al., 2014).

Based on the criteria for the classification of pathogenic mt-mRNA variants(Wong et al., 2020), evidence supporting the pathogenicity of the novel m.3955G>A variant is as follows. The variant was not found in our in-house Chinese (> 900 mtDNA sequences) or European (20,507 mtDNA sequences) databases, and was not related to human mitochondrial disorders in the Mitomap database

(http://www.mitomap.org/). The variant has been reported only once in cancer cells, in which it was predicted to decrease CI activity(Koshikawa et al., 2017). The *de novo* variant was not detected in the asymptomatic maternal relatives of the two patients. The variant, in which a highly conserved alanine (nonpolar/hydrophobic) is changed to threonine (polar/hydrophilic), is predicted to be "probably damaging" based on various *in silico* approaches and may result in conformational and functional changes in MT-ND1. The biochemical evidence of marked CI deficiency in cybrid cells was consistent with the location of the variant in *MT-ND1*. The most important evidence is that reduced levels of MT-ND1 protein and mature CI as well as mitochondrial dysfunction were only observed in mutant cybrids, excluding the involvement of nuclear variants and confirming the pathogenicity of the m.3955 G>A variant.

With recent advances in the technology for separating mitochondrial proteins and reconstructing complex structures based on electron microscopy, it has been found that every subunit of the MRC complexes is tightly connected(Porras et al., 2015; Fedor et al., 2017; Lobo-Jarne et al., 2018). CI participates in the initial step in the electron transfer chain and cooperates with numerous assembly factors(Vartak et al., 2014; Gorman et al., 2015). Variants in several subunits of CI, including MT-ND1, may result in markedly reduced levels of the fully assembled holoenzyme and negatively affect cellular energy metabolism(Gershoni et al., 2010). Biochemical disorders in oxidative phosphorylation result in proton leakage across the inner membrane and electron leakage from the electron transport chain, which causes the overproduction of ROS and a reduction in MMP(Hayashi et al., 2015; Porras et al., 2015; Zhao et al., 2019).

These results are in agreement with our study, as we found that the novel m.3955G>A variant in *MT-ND1* affected the complete assembly of CI and led to mitochondrial dysfunction. The basal, ATP-linked, reserve capacity and maximal OCRs as well as the CI activities were significantly reduced in the mutant cybrid cells compared with the WT cells. Significant increases in the ROS level and a significant reduction in MMP were also observed in the mutant cybrid cells. A combination of mitochondrial ROS overproduction and MMP collapse may release apoptotic factors and promote cell death(Murphy, 2016). Taken together, the deleterious effects of the m.3955G>A variant may include the downregulation of MT-ND1 expression and CI assembly, thus impairing oxidative phosphorylation and resulting in widespread mitochondrial dysfunction and cell death.

Although *MT-ND1* is a mutational hot spot for Leber hereditary optic neuropathy(Zhou et al., 2012; Zhang et al., 2014; Scheffler, 2015), LS or Leigh-like phenotypes have been reported in four families (six cases) harboring the variants m.3688G>A, m.3697G>A, m.3890G>A, and m.4171G>A(Moslemi et al., 2008; Valente et al., 2009; La Morgia et al., 2014; Negishi et al., 2014). The clinical phenotypes of the six reported cases are summarized in Table 2. Most of these LS and Leigh-like-associated variants exhibited homoplasmic inheritance, whereas our case is the second report of a heteroplasmic *MT-ND1* variant with an LS phenotype. Our patients experienced earlier disease onset and more severe seizures compared with the other reported cases, suggesting a probable greater impact of the m.3955G>A variant on protein function.

In conclusion, we provide conclusive evidence that m.3955G>A (p.A217T) in *MT-ND1* is a causative variant for LS, with our findings demonstrating the molecular pathomechanisms of this variant.

Acknowledgments

The authors thank the patients and their families.

Authors' contributions

All authors contributed to acquisition and interpretation of data, and approved the final manuscript. M.X drafting of the original manuscript. F.F designed the studies and supervised the work. F.F, H.P, and ME revised the manuscript.

Declaration of Competing Interests

The authors declare no known competing financial interests or personal relationships that could influence the work reported in this paper.

Ethical approval

The study was approved by the Local Ethics committee of Beijing Children's Hospital (2014-10).

Patient consent statement

Informed written consent from the patient's parents was obtained for the publication of clinical information.

Data availability statement

The data that support the findings of this study are available from the corresponding author on reasonable request.

References

Adzhubei, I., Jordan, D.M., Sunyaev, S.R., 2013. Predicting functional effect of human missense mutations using PolyPhen-2. Current protocols in human genetics Chapter 7, Unit7.20.

Arii, J., Tanabe, Y., 2000. Leigh syndrome: serial MR imaging and clinical follow-up. AJNR Am J Neuroradiol 21, 1502-1509.

Baertling, F., Rodenburg, R.J., Schaper, J., Smeitink, J.A., Koopman, W.J., Mayatepek, E., Morava, E., Distelmaier, F., 2014. A guide to diagnosis and treatment of Leigh syndrome. Journal of neurology, neurosurgery, and psychiatry 85, 257-265.

Choi, Y., Chan, A.P., 2015. PROVEAN web server: a tool to predict the functional effect of amino acid substitutions and indels. Bioinformatics 31, 2745-2747.

Chomyn, A., 1996. Platelet-mediated transformation of human mitochondrial DNA-less cells. Methods in enzymology 264, 334-339.

Delmiro, A., Rivera, H., García-Silva, M.T., García-Consuegra, I., Martín-Hernández, E., Quijada-Fraile, P., de Las Heras, R.S., Moreno-Izquierdo, A., Martín, M., Arenas, J., Martínez-Azorín, F., 2013. Whole-exome sequencing identifies a variant of the mitochondrial MT-ND1 gene associated with epileptic encephalopathy: west syndrome evolving to Lennox-Gastaut syndrome. Human mutation 34, 1623-1627.

Fedor, J.G., Jones, A.J.Y., Di Luca, A., Kaila, V.R.I., Hirst, J., 2017. Correlating kinetic and structural data on ubiquinone binding and reduction by respiratory complex I. Proceedings of the National Academy of Sciences of the United States of America 114, 12737-12742.

Gershoni, M., Fuchs, A., Shani, N., Fridman, Y., Corral-Debrinski, M., Aharoni, A., Frishman, D., Mishmar, D., 2010. Coevolution predicts direct interactions between mtDNA-encoded and nDNA-encoded subunits of oxidative phosphorylation complex i. Journal of molecular biology 404, 158-171.

Gorman, G.S., Blakely, E.L., Hornig-Do, H.T., Tuppen, H.A., Greaves, L.C., He, L., Baker, A., Falkous, G., Newman, J., Trenell, M.I., Lecky, B., Petty, R.K., Turnbull, D.M., McFarland, R., Taylor, R.W., 2015. Novel MTND1 mutations

cause isolated exercise intolerance, complex I deficiency and increased assembly factor expression. Clinical science (London, England : 1979) 128, 895-904.

Grady, J.P., Pickett, S.J., Ng, Y.S., Alston, C.L., Blakely, E.L., Hardy, S.A., Feeney, C.L., Bright, A.A., Schaefer, A.M., Gorman, G.S., McNally, R.J., Taylor, R.W., Turnbull, D.M., McFarland, R., 2018. mtDNA heteroplasmy level and copy number indicate disease burden in m.3243A>G mitochondrial disease. EMBO molecular medicine 10.

Hayashi, G., Cortopassi, G., 2015. Oxidative stress in inherited mitochondrial diseases. Free radical biology & medicine 88, 10-17.

Ji, K., Wang, W., Lin, Y., Xu, X., Liu, F., Wang, D., Zhao, Y., Yan, C., 2020. Mitochondrial encephalopathy Due to a Novel Pathogenic Mitochondrial tRNA(Gln) m.4349C>T Variant. Annals of clinical and translational neurology 7, 980-991.

Ji, K., Zheng, J., Sun, B., Liu, F., Shan, J., Li, D., Luo, Y.B., Zhao, Y., Yan, C., 2014. Novel mitochondrial C15620A variant may modulate the phenotype of mitochondrial G11778A mutation in a Chinese family with Leigh syndrome. Neuromolecular medicine 16, 119-126.

Jia, Z., Zhang, Y., Li, Q., Ye, Z., Liu, Y., Fu, C., Cang, X., Wang, M., Guan, M.X., 2019. A coronary artery disease-associated tRNAThr mutation altered mitochondrial function, apoptosis and angiogenesis. Nucleic acids research 47, 2056-2074.

Koshikawa, N., Akimoto, M., Hayashi, J.I., Nagase, H., Takenaga, K., 2017. Association of predicted pathogenic mutations in mitochondrial ND genes with distant metastasis in NSCLC and colon cancer. Sci Rep 7, 15535.

Kremer, L.S., Prokisch, H., 2017. Identification of Disease-Causing Mutations by Functional Complementation of Patient-Derived Fibroblast Cell Lines. Methods Mol Biol 1567, 391-406.

La Morgia, C., Caporali, L., Gandini, F., Olivieri, A., Toni, F., Nassetti, S., Brunetto, D., Stipa, C., Scaduto, C., Parmeggiani, A., Tonon, C., Lodi, R., Torroni, A., Carelli, V., 2014. Association of the mtDNA m.4171C>A/MT-ND1 mutation with

both optic neuropathy and bilateral brainstem lesions. BMC Neurol 14, 116.

Lake, N.J., Compton, A.G., Rahman, S., Thorburn, D.R., 2016. Leigh syndrome: One disorder, more than 75 monogenic causes. Annals of neurology 79, 190-203.

Lightowlers, R.N., Taylor, R.W., Turnbull, D.M., 2015. Mutations causing mitochondrial disease: What is new and what challenges remain? Science 349, 1494-1499.

Lobo-Jarne, T., Ugalde, C., 2018. Respiratory chain supercomplexes: Structures, function and biogenesis. Seminars in cell & developmental biology 76, 179-190.

Moslemi, A.R., Darin, N., Tulinius, M., Wiklund, L.M., Holme, E., Oldfors, A., 2008. Progressive encephalopathy and complex I deficiency associated with mutations in MTND1. Neuropediatrics 39, 24-28.

Murphy, M.P., 2016. Understanding and preventing mitochondrial oxidative damage. Biochemical Society transactions 44, 1219-1226.

Negishi, Y., Hattori, A., Takeshita, E., Sakai, C., Ando, N., Ito, T., Goto, Y., Saitoh, S., 2014. Homoplasmy of a mitochondrial 3697G>A mutation causes Leigh syndrome. J Hum Genet 59, 405-407.

Ogawa, E., Shimura, M., Fushimi, T., Tajika, M., Ichimoto, K., Matsunaga, A., Tsuruoka, T., Ishige, M., Fuchigami, T., Yamazaki, T., Mori, M., Kohda, M., Kishita, Y., Okazaki, Y., Takahashi, S., Ohtake, A., Murayama, K., 2017. Clinical validity of biochemical and molecular analysis in diagnosing Leigh syndrome: a study of 106 Japanese patients. J Inherit Metab Dis 40, 685-693.

Parey, K., Wirth, C., Vonck, J., Zickermann, V., 2020. Respiratory complex I - structure, mechanism and evolution. Current opinion in structural biology 63, 1-9.

Pejaver, V., Urresti, J., Lugo-Martinez, J., Pagel, K.A., Lin, G.N., Nam, H.J., Mort, M., Cooper, D.N., Sebat, J., Iakoucheva, L.M., Mooney, S.D., Radivojac, P., 2020. Inferring the molecular and phenotypic impact of amino acid variants with MutPred2. Nature communications 11, 5918.

Porras, C.A., Bai, Y., 2015. Respiratory supercomplexes: plasticity and implications. Frontiers in bioscience (Landmark edition) 20, 621-634.

Qian, W., Kumar, N., Roginskaya, V., Fouquerel, E., Opresko, P.L., Shiva, S., Watkins,

S.C., Kolodieznyi, D., Bruchez, M.P., Van Houten, B., 2019. Chemoptogenetic damage to mitochondria causes rapid telomere dysfunction. Proceedings of the National Academy of Sciences of the United States of America 116, 18435-18444.

Rahman, J., Noronha, A., Thiele, I., Rahman, S., 2017. Leigh map: A novel computational diagnostic resource for mitochondrial disease. Annals of neurology 81, 9-16.

Scheffler, I.E., 2015. Mitochondrial disease associated with complex I (NADH-CoQ oxidoreductase) deficiency. J Inherit Metab Dis 38, 405-415.

Sofou, K., De Coo, I.F., Isohanni, P., Ostergaard, E., Naess, K., De Meirleir, L., Tzoulis, C., Uusimaa, J., De Angst, I.B., Lonnqvist, T., Pihko, H., Mankinen, K., Bindoff, L.A., Tulinius, M., Darin, N., 2014. A multicenter study on Leigh syndrome: disease course and predictors of survival. Orphanet J Rare Dis 9, 52.

Valente, L., Piga, D., Lamantea, E., Carrara, F., Uziel, G., Cudia, P., Zani, A., Farina, L., Morandi, L., Mora, M., Spinazzola, A., Zeviani, M., Tiranti, V., 2009. Identification of novel mutations in five patients with mitochondrial encephalomyopathy. Biochim Biophys Acta 1787, 491-501.

Vartak, R.S., Semwal, M.K., Bai, Y., 2014. An update on complex I assembly: the assembly of players. Journal of bioenergetics and biomembranes 46, 323-328.

Wong, L.C., Chen, T., Schmitt, E.S., Wang, J., Tang, S., Landsverk, M., Li, F., Zhang, S., Wang, Y., Zhang, V.W., Craigen, W.J., 2020. Clinical and laboratory interpretation of mitochondrial mRNA variants. Human mutation.

Zhang, J., Jiang, P., Jin, X., Liu, X., Zhang, M., Xie, S., Gao, M., Zhang, S., Sun, Y.H., Zhu, J., Ji, Y., Wei, Q.P., Tong, Y., Guan, M.X., 2014. Leber's hereditary optic neuropathy caused by the homoplasmic ND1 m.3635G>A mutation in nine Han Chinese families. Mitochondrion 18, 18-26.

Zhao, X., Cui, L., Xiao, Y., Mao, Q., Aishanjiang, M., Kong, W., Liu, Y., Chen, H., Hong, F., Jia, Z., Wang, M., Jiang, P., Guan, M.X., 2019. Hypertension-associated mitochondrial DNA 4401A>G mutation caused the aberrant processing of tRNAMet, all 8 tRNAs and ND6 mRNA in the light-strand transcript. Nucleic acids research 47, 10340-10356.

Zhou, X., Qian, Y., Zhang, J., Tong, Y., Jiang, P., Liang, M., Dai, X., Zhou, H., Zhao, F., Ji, Y., Mo, J.Q., Qu, J., Guan, M.X., 2012. Leber's hereditary optic neuropathy is associated with the T3866C mutation in mitochondrial ND1 gene in three Han Chinese Families. Invest Ophthalmol Vis Sci 53, 4586-4594.

Zickermann, V., Wirth, C., Nasiri, H., Siegmund, K., Schwalbe, H., Hunte, C., Brandt, U., 2015. Structural biology. Mechanistic insight from the crystal structure of mitochondrial complex I. Science 347, 44-49.

Figure legends

Fig 1 Clinical images of the patient 1. A. Brain MRI of patient 1 showed bilateral symmetrical lesions (red arrows) with increased T2 signals in brainstem, basal ganglia and thalamus at 7 months of age (*i-ii*) and 4.5 years of age (*iii-iv*). Images *iii* and *iv* also exhibited cerebral atrophy. **B**. The EEG of patient 1 at 4.5 years of age recorded multifocal high-amplitude epileptic discharges (*i*) and a seizure episode (*ii*).

Fig 2 Clinical images of the patient 2. A. Brain MRI of patient 2 at 5 months of age exhibited bilateral symmetrical lesions (red arrows) in brainstem, basal ganglia and thalamus in T2-Flair (*i-ii*) and diffusion weighted imaging (*iii-iv*). Abnormal signals were also detected in the frontotemporal lobe (yellow arrow) on T2/Flair images (*ii*). **B**. The EEG of patient 2 at 5 months recorded hypsarrhythmia and burst suppression pattern (*i*) and an episode of spasm (*ii*).

Fig 3 Molecular genetic assays. A. Family pedigrees of patient 1 (*i*) and patient 2 (ii) (arrows indicate the probands). ND, not detected. **B**. Phylogenetic conservation of the human MT-ND1 (arrow indicates the p.A217T variant). **C.** The predicted impact of m.3955G>A variant on protein structure. (i) The overview of CI. (ii) The MT-ND1 protein as a ribbon representation and the residue A217 in red. (iii-iv) Detailed view of the environments of A217(iii) and A217T (iv) where the residues are colored in red and represented as sticks. The hydrogen bonds with neighbor atoms are indicated with yellow dashed lines.

Fig 4 Effects of the m.3955G>A variant on mitochondrial proteins. A. Relative MT-ND1 protein levels in cybrid cell lines wild-type, M1, and M2 determined by Western

blotting. VDAC was used as the internal control. **B.** The expression of MT-ND1 protein in the fibroblast cells derived from patient 1 and his mother determined by Western blotting. VDAC was used as the internal control. **C.** The expression of levels of MT-ND4, MT-ND5 (mtDNA-encoded CI subunits) and NDUFB8 (nDNA-encoded CI subunit) were evaluated by Western blotting. VDAC was used as the internal control. **D.** For cybrids cell lines wild-type, M1, and M2, Blue native PAGE/immunoblot analysis of MRC complexes using antibodies against subunits of complexes I (NDUFS2), II (SDHA), III (UQCRC2), IV (COXIV), and V (ATPB). VDAC was used as the internal control. CI, complex I; CII, complex II; CIII, complex III; CIV, complex IV; CV, complex V; SC, supercomplex.

Fig 5 The m.3955G>A variant results in mitochondrial respiration deficiency. A. Analysis of OCRs in wild-type, M1, and M2 cybrid cell lines using the inhibitors oligomycin, FCCP, antimycin A, and rotenone. The basal OCR, ATP-linked OCR, Proton leakage, maximal OCR, reserve capacity OCR and non-mitochondrial OCR in cybrid cells are shown. Values are means ± SD. *$p < 0.05$ by one-way ANOVA. **B.** Analysis of complex I-, II-, and IV-mediated OCRs in wild-type, M1, and M2 cybrid cells. Values are means ± SD. *$p < 0.05$ by one-way ANOVA.

Fig 6 ROS production in WT, M1, and M2 cybrid cells. **A**. Representative images of Hochest staining, Mitotracker staining, MitoSOX staining and merged images of both in cybrid cells. **B**. The relative ratios of fluorescence intensity were calculated. Values are means ± SD. *$p < 0.05$ by one-way ANOVA.

Fig 7 MMP in WT, M1, and M2 cybrid cells. **A**. The representative images of Hochest staining, JC-1 aggregates, JC-1 monomers and merged images of those in cybrid cells.

B. The relative ratio of JC-1 aggregates to JC-1 monomers (ratio of 590/530 nm emission intensity) was calculated. Values are means ± SD. *$p < 0.05$ by one-way ANOVA.

Figure 1

Click here to access/download;Figure;Figure_1_ND1.pdf

Fig. 1

A

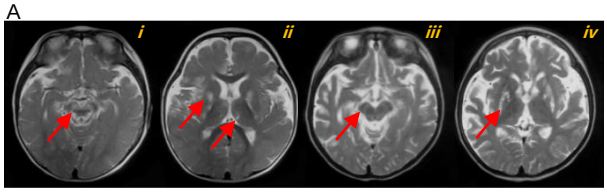

B

Figure 2

Click here to access/download;Figure;Figure_2_ND1.pdf

Fig. 2

A

B

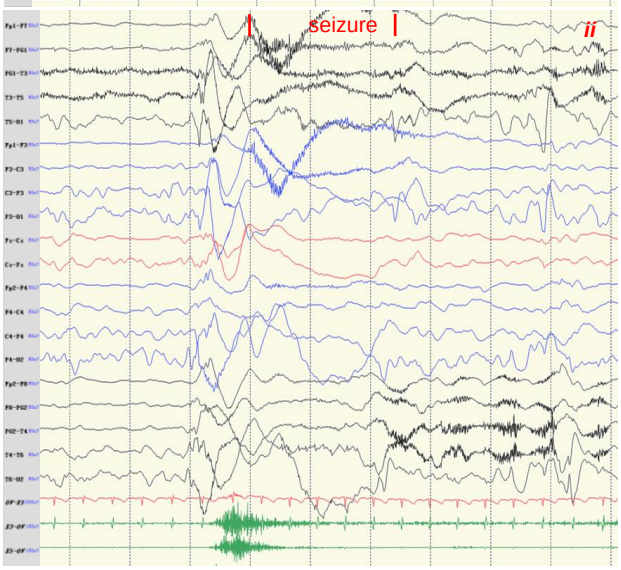

Fig. 3

A

i

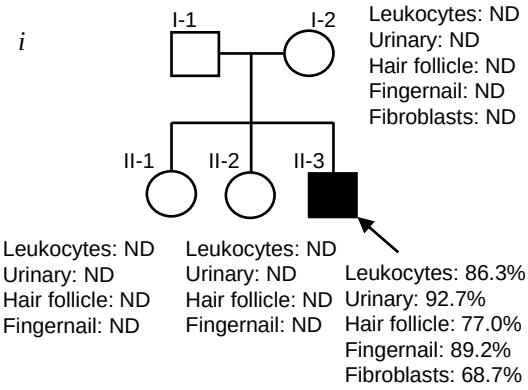

ii

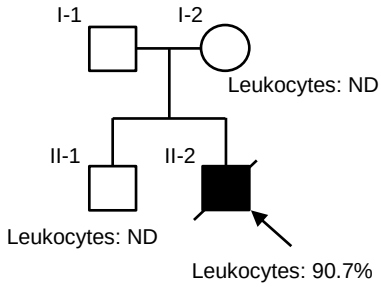

B

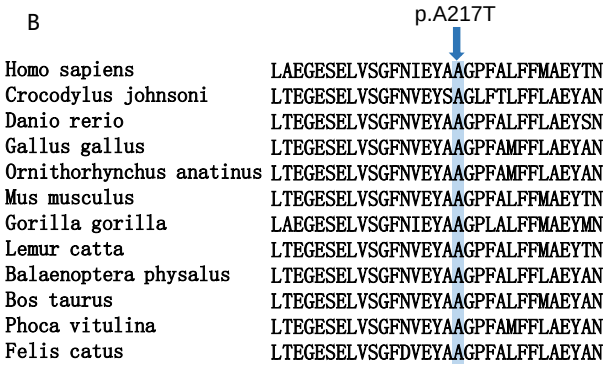

C

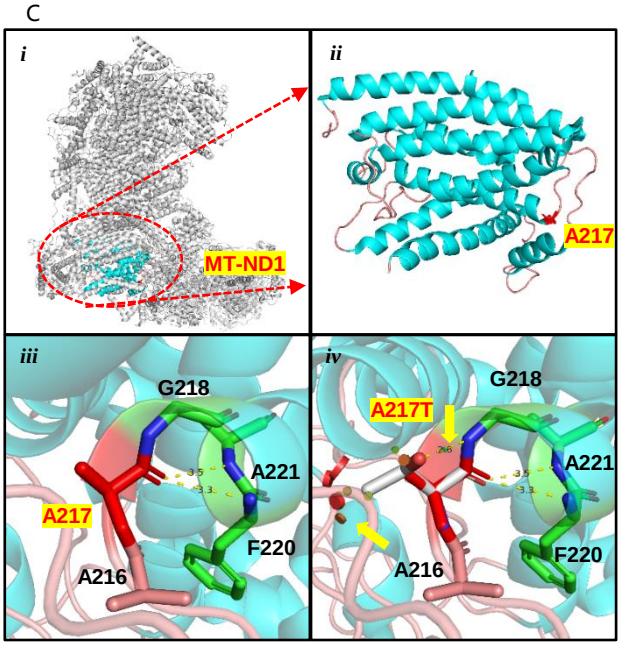

Figure 4rv

Click here to access/download;Figure;T-Figure4_ND1 - rv.pdf

Fig.4

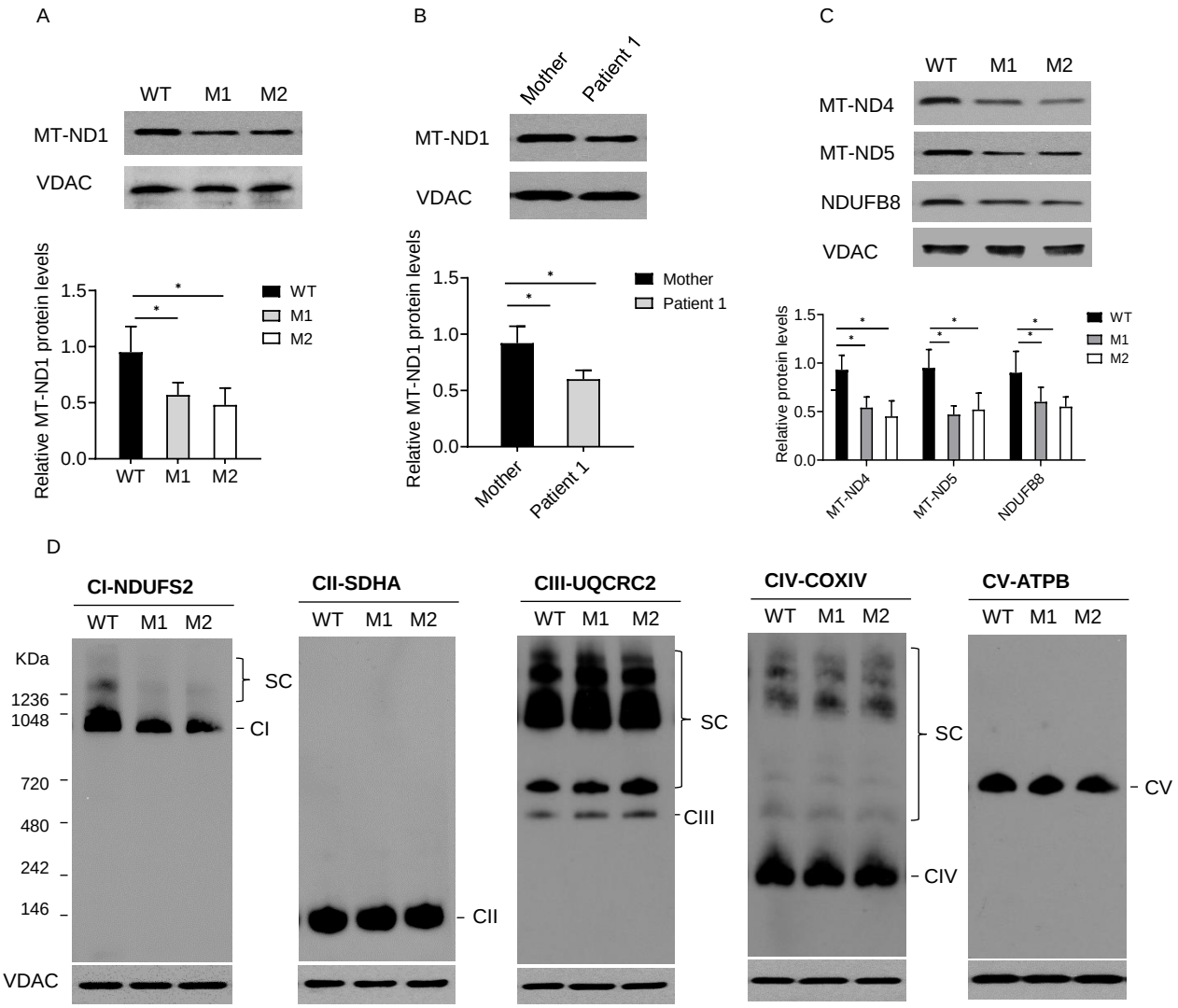

Figure 5

Click here to access/download;Figure;Figure_5_ND1.pdf

Fig.5

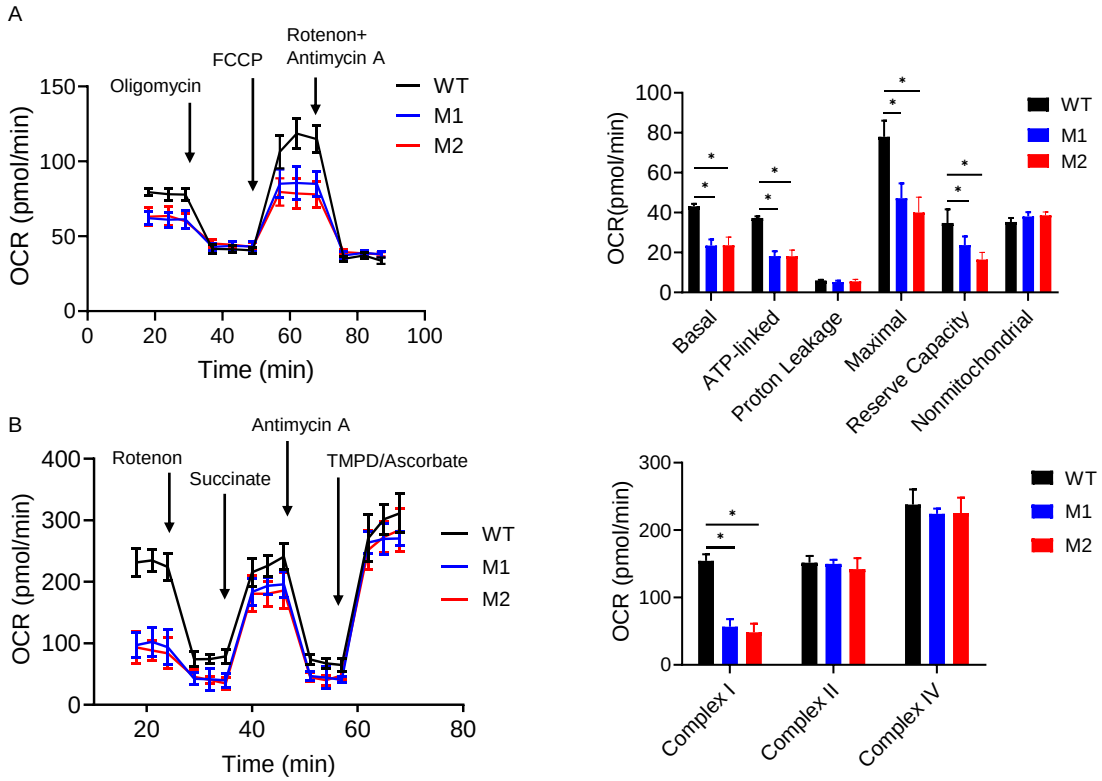

Figure 6rv

Click here to access/download;Figure;T-Figure6_ND1 - rv.pdf

Fig.6

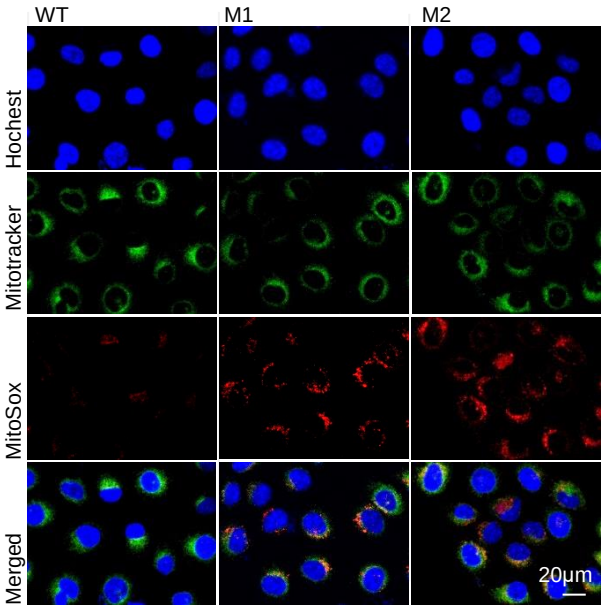

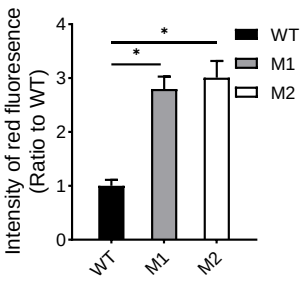

Figure 7rv

Click here to access/download;Figure;T-Figure7_ND1 - rv.pdf

Fig.7

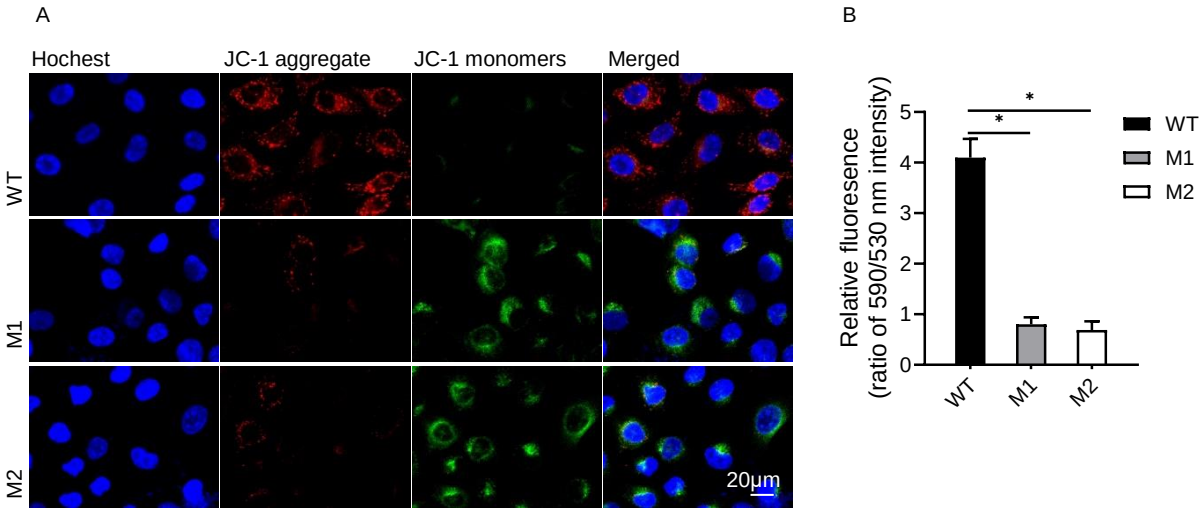

Table 1. MRC enzyme analyses in mutant and wild-type cybrid cells.

	CI	CII	CII+III	CIII	CIV
Cybrid cell M1					
% of CS	**34.3±5.6**	103.7±3.7	87.9±9.1	112.1±8.3	124.5±4.8
% of CII	**29.1±6.7**	-	91.2±4.9	106.7±7.4	114.5±7.6
Cybrid cell M2					
% of CS	**28.4±5.6**	99.2±2.4	85.6±7.2	112.1±8.3	124.5±4.8
% of CII	**27.0±7.1**	-	89.6±6.2	103.2±5.2	106.5±8.5
Cybrid cell WT					
% of CS	94.2±8.5	89.7±9.7	97.4±10.1	104.6±7.9	96.1±8.5
% of CII	97.4±7.1	-	90.8±9.0	97.3±8.3	91.5±6.1

CI, complex I; CII, complex II; CIII, complex III; CIV, complex IV; CS, citrate synthase. Relative enzyme activities is calculated as percentages of mean values relative to CS and CII.

Values in bold indicate a deficiency of the MRC complex activity.

Table 2. A summary of patients with LS/Leigh like Syndrome reported in the literature with pathogenic variants in *MT-ND1*

	Family 1	Family 2	Family 3	Family 4			Family 5	Family 6
	Patient 1	Patient 2	Patient 3	Patient 4	Patient 5	Patient 6	Patient 7	Patient 8
gene variants	m.3955G>A	m.3955G>A	m.3688G>A	m.3697G>A	m.3697G>A	m.3697G>A	m.3890G>A	m.4171C>A
amino acid change	p.A217T	p.A217T	p.A128T	p.G131S	p.G131S	p.G131S	p.R195Q	p.L289M
homoplasmy /heteroplasmy	heteroplasmy	heteroplasmy	homoplasmy	homoplasmy	homoplasmy	homoplasmy	heteroplasmy	homoplasmic
mutation loads	86.3% in leukocytes and 92.7% in urinary	90.7% in leukocytes					95% in muscle	
phenotype	LS	LS	LS	LS	LS	LS	LS	LHON and Leigh like syndrome
clinical presentation								
age at onset	7 months	5 months	10 months	1.5 years	2 years	1.5 years	2 years	12 years
sex	male	male	male	female	male	female	female	male
perinatal period	-	-	-	-	-	-	premature birth (33w) and SGA	-
psychomotor retardation	-	+	-	-	-	-	+	-
psychomotor regression	+	+	+	+	+	+	+	+
metabolic failure	-	-	+	-	-	-	-	-
ophthalmology abnormalities	-	ND	strabismus	-	-	-	-	nystagmus;visual loss;optic atrophy
seizures	+	+	+	-	-	-	-	-
dystonia	+	+	+	+	+	+	-	+
hearing loss	-	-	-	+	-	-	-	-

	Family 1	Family 2	Family 3	Family 4			Family 5	Family 6
	Patient 1	Patient 2	Patient 3	Patient 4	Patient 5	Patient 6	Patient 7	Patient 8
apnea	+	-	-	-	-	-	+	-
respiratory failure	-	-	-	-	-	+	+	-
elevated lactic acid	+ /CSF	+ /serum	+ /serum	- /CSF	- /CSF	- /CSF	+ /CSF; serum	+ /serum
investigations								
basal ganglia	symmetric leisions	symmetric leisions	symmetric leisions	symmetric leisions	symmetric leisions	symmetric leisions	symmetric leisions	symmetric leisions
brain stem	symmetric leisions	symmetric leisions	symmetric leisions	-	-	symmetric leisions	symmetric leisions	symmetric leisions
brain cortex	+	+	+	-	-	-	-	-
subcortical white matter	-	-	+	-	-	-	-	-
lactate peak in MRS	ND	ND	+	ND	ND	ND	ND	ND
muscle biopsy	-	-	-	-	-	-	type 2 fiber atrophy	ND
literature citation	current /2021	current /2021	2009	2014	2014	2014	2008	2014

SGA: small for gestational age; ND: not determined; LHON: Leber Hereditary Optic Neuropathy; LS: Leigh Syndrome.